Neuropharmacology 242 (2024) 109759

Contents lists available at ScienceDirect

Neuropharmacology

journal homepage: www.elsevier.com/locate/neuropharm

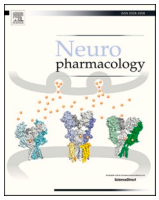

CHIR99021 causes inactivation of Tyrosine Hydroxylase and depletion of dopamine in rat brain striatum

Sally Hamdon [a,b], Pol Fernandez-Gonzalez [a], Muhammad Yusof Omar [a,b], Marta González-Sepúlveda [c,d], Jordi Ortiz [a,b,e,1], Carles Gil [a,b,*,1]

[a] Department of Biochemistry and Molecular Biology, Universitat Autònoma de Barcelona, Spain
[b] Institut de Neurociències, Universitat Autònoma de Barcelona, Spain
[c] Neurodegenerative Diseases Research Group, Vall d'Hebron Research Institute (VHIR) - Center for Networked Biomedical Research on Neurodegenerative Diseases (CIBERNED), 08035, Barcelona, Spain
[d] Aligning Science Across Parkinson's (ASAP) Collaborative Research Network, Chevy Chase, MD, 20815, USA
[e] Centro Investigación Biomédica en Red de Salud Mental, CIBERSAM, and Translational Neuroscience Unit, Parc Taulí University Hospital and Universitat Autònoma de Barcelona, Spain

ARTICLE INFO

Handling Editor: Dr J Young

Keywords:
Dopamine
Tyrosine Hydroxylase
Striatum
GSK3
HPLC
CHIR99021

ABSTRACT

CHIR99021, also known as laduviglusib or CT99021, is a Glycogen-synthase kinase 3β (GSK3β) inhibitor, which has been reported as a promising drug for cardiomyocyte regeneration or treatment of sensorial hearing loss. Since the activation of dopamine (DA) receptors regulates dopamine synthesis and they can signal through the β-arrestin pathway and GSK3β, we decided to check the effect of GSK3β inhibitors (CHIR99021, SB216763 and lithium ion) on the control of DA synthesis. Using *ex vivo* experiments with minces from rat brain striatum, we observed that CHIR99021, but not SB216763 or lithium, causes complete abrogation of both DA synthesis and accumulation, pointing to off-target effects of CHIR99021. This decrease can be attributed to tyrosine hydroxylase (TH) inhibition since the accumulation of L-DOPA in the presence of a DOPA decarboxylase inhibitor was similarly decreased. On the other hand, CHIR99021 caused a dramatic increase in the DOPAC/DA ratio, an indicator of DA metabolization, and hindered DA incorporation into striatum tissue. Tetrabenazine, an inhibitor of DA vesicular transport, also caused DA depletion and DOPAC/DA ratio increase to the same extent as CHIR99021. In addition, both CHIR99021 or SB216763, but not lithium, decreased TH phosphorylation in Ser19, but not in Ser31 or Ser40. These results demonstrate that CHIR99021 can lead to TH inactivation and DA depletion in brain striatum, opening the possibility of its use in DA-related disorders, and shows effects to be considered in future clinical trials. More work is needed to find the mechanism exerted by CHIR99021 on DA accumulation.

1. Introduction

Dopamine (DA) transmission is described as essential in the control of behavior through natural rewards, such as food, sex, and nurture (Spanagel and Weiss, 1999). Moreover, dysregulation of DA metabolism is a key event in neurodegenerative diseases, such as Parkinson's disease (PD) (Johnson et al., 2018) or in mental disorders, such as schizophrenia (Bird et al., 1979; Mackay et al., 1982), addiction (Koob and Volkow, 2010) or depression (Duda et al., 2020). Additionally, due to the role of DA in the control of coordinated movements, alterations in the dopaminergic system also contribute to diseases causing locomotion impairment (Smith-Dijak et al., 2019). DA is synthesized by tyrosine hydroxylase (TH; tyrosine 3-monooxygenase; E.C. 1.14.16.2) and DOPA decarboxylase, and it is rapidly internalized into synaptic vesicles by means of the vesicular monoamine transporter 2 (VMAT2) to prevent its auto-oxidation (Gonzalez-Sepulveda et al., 2023) and to prepare

Abbreviations: DA, dopamine; L-DOPA, levodopa; DOPAC, 3,4-dihydroxyphenylacetic acid; TH, tyrosine hydroxylase; VMAT2, vesicular monoamine transporter 2; TBZ, tetrabenazine; GSK3, Glycogen-synthase kinase.

* Corresponding author. Department of Biochemistry and Molecular Biology, School of Medicine, and Institut de Neurociències, Universitat Autònoma de Barcelona, 08193, Bellaterra, Cerdanyola del Vallès, Catalonia, Spain.
E-mail address: carles.gil@uab.cat (C. Gil).
[1] Contributed equally.

https://doi.org/10.1016/j.neuropharm.2023.109759
Received 3 July 2023; Received in revised form 6 October 2023; Accepted 9 October 2023
Available online 14 October 2023

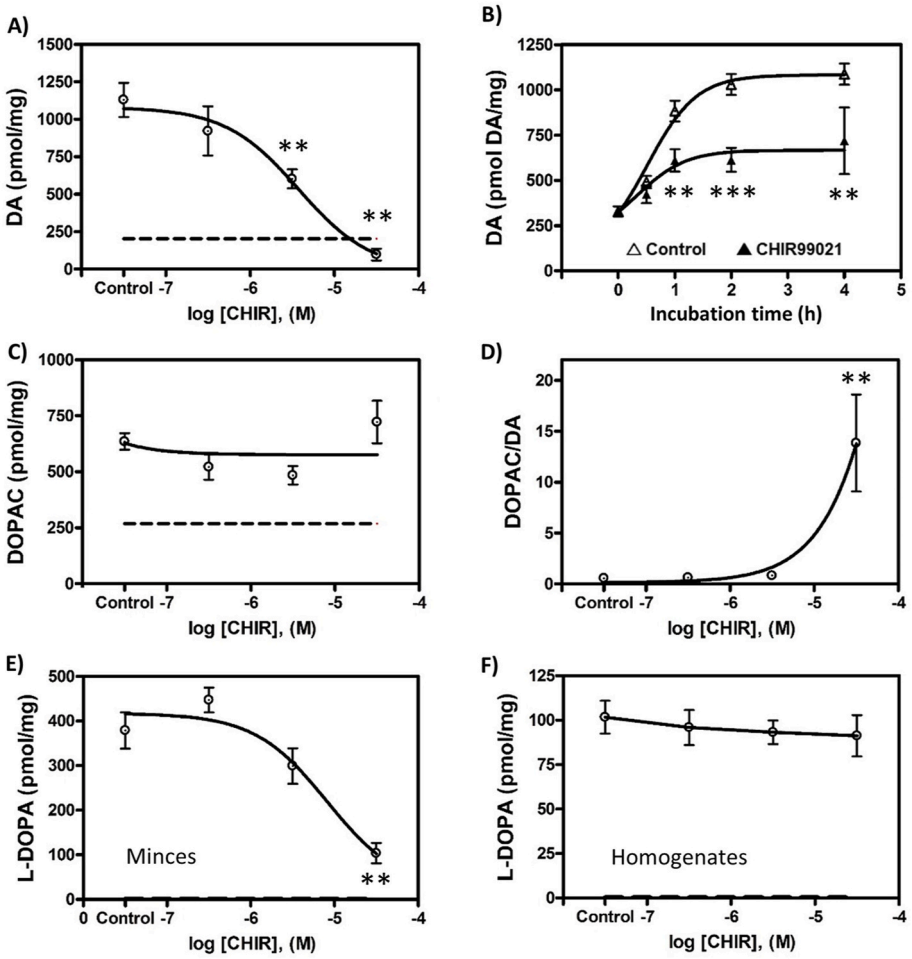

Fig. 1. Effects of CHIR99021 on dopamine accumulation and metabolism in rat brain striatal minces. (A) Concentration-response curve of CHIR99021 in striatal minces *ex vivo*, measuring dopamine (DA) accumulation over a 2h incubation period, using concentrations of 0.3, 3 and 30 μM CHIR99021 or control without CHIR99021 (six incubates per group obtained from a single animal, n = 6). Basal DA was measured as control samples placed on ice during the 2h incubation period (six incubates, dashed line). **(B)** Time-response curve of DA accumulation in striatal minces *ex vivo* with 3 μM CHIR99021 for 30 min, 1h, 2h, 4h (n = 6, black triangles) and controls with vehicle (n = 6, white triangles) for each incubation period. Controls were treated with the corresponding concentration of DMSO used to dissolve CHIR99021 (n = 6), and basal dopamine measured the same as in A) and represented as 0 time (n = 6). The same protocol as in A was used in striatal minces to determine DOPAC **(C).** The DOPAC/DA ratio was calculated **(D).** The L-DOPA levels after CHIR99021 treatment were measured in minces **(E)** and in homogenates **(F)** from striatal minces. In the L-DOPA determinations, 100 μM NSD-1015 was also added at the beginning of the experiment. Data are expressed as mean ± SEM for each group, CHIR99021 *vs* control, one-way ANOVA followed by Dunnett's post-hoc test for dose-response graphs and two-way ANOVA followed by Bonferroni's post-hoc test for time-response graph. $^{**}p < 0.01$, $^{***}p < 0.001$. Sigmoidal dose-response curve regression was used in every case to create the adjusted curves.

synaptic release (Meiser et al., 2013). Cytosolic DA can also be metabolized to different compounds including 3,4-dihydroxyphenylacetic acid (DOPAC). Therefore, the ratio between DOPAC and DA levels is usually considered an index of DA metabolism. As an imbalance of brain DA levels could lead to numerous diseases, TH is subjected to an intense regulation. Short-term modulation of TH activity includes end-product feedback inhibition by DA (González-Sepúlveda et al., 2022) and phosphorylation at serine residues Ser8, Ser19, Ser31 and Ser40 (Dunkley and Dickson, 2019). Several studies showed that increased phosphorylation at Ser40 positively correlated with TH activity (Bobrovskaya et al., 2007), while phosphorylation of Ser19 and Ser31 increases the rate of phosphorylation of Ser40 and potentiates TH activation (Lehmann et al., 2006). DA exerts its functions through membrane receptors, which comprise two classes: the D1-like class (D1 and D5) and the D2-like class (D2, D3 and D4) (Jaber et al., 1996). Both classes of receptors are seven transmembrane proteins which can act by two pathways, one inhibits intracellular cAMP *via* protein G_i while the other can initiate a cAMP-independent pathway by promoting a scaffolding complex that leads to the activation of both ERK1/2 and GSK3β signaling, through the recruitment of β-arrestin (Bibb, 2005). These two pathways are differently turned-on depending on the ligand, in a phenomenon known as biased agonism (Smith et al., 2018).

CHIR99021 (also known as laduviglusib or CT99021) is a GSK3β inhibitor which is currently in clinical phase 2b for the restoration of some types of hearing loss (McLean et al., 2021; ClinicalTrials.gov Identifier: NCT05086276) and is a promising molecule that has also been successfully tested in inhibition of adipogenesis (Bennett et al., 2002), coronary and myocardial diseases (Badimon et al., 2019; Xu et al., 2022), cancer (Oh et al., 2017; Lee et al., 2018; Houben et al., 2022), lung repair therapy (Uhl et al., 2015), stimulation of stem cells (Zhao et al., 2014), and type II diabetes mellitus (Ring et al., 2003). Moreover, CHIR99021 has also recently been proposed as a potential drug for Huntington's disease (Hu et al., 2021).

In the present work *ex vivo* assays with rat brain striatum tissue were used to study the effects of three GSK3β inhibitors (CHIR99021, SB216763 and lithium) on DA metabolism. The results obtained demonstrate that CHIR99021 indirectly inhibits TH and depletes DA in brain striatum samples and should be considered as a potential drug for the treatment of disorders caused by overproduction of DA. The exact mechanism by which CHIR99021 impairs DA accumulation is still

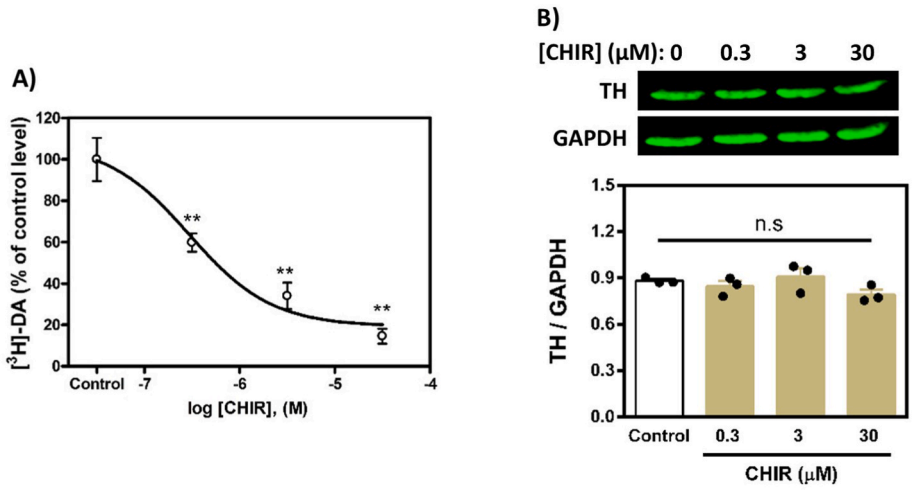

Fig. 2. CHIR99021 inhibits tyrosine hydroxylase enzymatic activity. (A) Concentration-response curve of CHIR99021 on striatal [^{3}H]-DA synthesis in minces *ex vivo* was measured after a preincubation period of 2 h. CHIR99021 was added using concentrations of 0.3, 3 and 30 μM (n = 6 per concentration) or control without CHIR (n = 6) 10 min before the end of preincubation. Then, [^{3}H]-tyrosine was added and incubated for 10 additional minutes. The curve is obtained by normalization of the data to percent of control. In all cases, data are expressed as mean ± SEM for each group. Asterisks indicate **p < 0.01 CHIR99021 vs control, one-way ANOVA followed by Dunnett's post-hoc test. The curve was adjusted to sigmoidal dose-response regression. **(B)** TH amount was assessed by western blot after treatment of minces with 0.3, 3 and 30 μM CHIR99021 or control without CHIR99021 (shown as 0), as in A. GAPDH amount was also detected by western blot and the TH/GAPDH ratio was calculated and is represented as a bar graph, which shows means and SEM, after one-way ANOVA analysis with Newman-Keuls post-test, which yielded non-significant results (n.s.) in every case. Bands from representative western blots are also shown.

unknown.

2. Materials and methods

2.1. Animals

Experiments were conducted with tissue from male Sprague-Dawley rats weighing 200–250g (from the Animal Service, Universitat Autònoma de Barcelona or from Charles River). Animals were housed five per cage with *ad libitum* access to food and water during a 12-h light/dark cycle. Protocols for animal use were approved by the Ethics Committee for Human and Animal Research (Universitat Autònoma de Barcelona) in accordance with guidelines established by the Ethical Committee for the Use of Laboratory Animals in Spain (53/2013) and the European Ethical Committee (2010/63/EU).

2.2. Preparation of striatal minces

Freshly obtained rat brains were chilled immediately in modified Krebs-Ringer-bicarbonate medium with the following composition: 120 mM NaCl, 0.8 mM KCl, 2.6 mM $CaCl_2$, 0.67 mM $MgSO_4$, 1.2 mM KH_2PO_4, 27.5 mM $NaHCO_3$, and 10 mM glucose, saturated with 95% O_2/5% CO_2 and adjusted to pH 7.4. Tissue extraction and handling were performed at 4 °C in a cold chamber. To obtain the dorsal/medial striata from both hemispheres, the brain was cut in half in the sagittal plane and the striata were visually exposed with forceps and peeled off. Thereafter, striata were sliced using a McIlwain tissue chopper, first longitudinally and then transversally, to obtain tissue minces (also known as miniprisms or slices) of 0.3 × 0.3 mm/side. Tissue miniprisms, or minces, is a system widely used to assess metabolism changes in *ex vivo* tissues (e.g., Tiger et al., 1989; Ma et al., 2014). Tissue minces were suspended in ice-cold Krebs Ringer bicarbonate medium, and washed three times by centrifugation (1,000g, 1 min, 4 °C), to remove debris of damaged cells, and resuspended. Striatal tissue from a single rat yielded up to 30 samples of 25 μL each of the settled minces suspension corresponding to 24 incubation samples and 6 blank samples (0.3–0.7 mg protein each). Under continuous and gentle stirring to assure homogeneity amongst samples and replicates, 2 mL of minces suspension were distributed into polypropylene tubes containing 225 μL of ice-cold Krebs Ringer bicarbonate medium. Blank tubes were kept on ice and the rest were incubated at 37 °C in soft agitation in an Eppendorf Thermomixer (5 Prime, Inc., Boulder, CO) in a 95% O_2/5% CO_2 atmosphere.

2.3. Determination of endogenous L-DOPA, DA and DOPAC levels by HPLC-EC

Levels of L-DOPA, DA and DOPAC were determined in striatal minces. After different incubation times, tissue minces were sonicated in 0.25 M perchloric acid containing 0.25 mM EDTA and 0.1 mM sodium metabisulphite. A 10-μL aliquot was taken for protein quantification by the BCA method (Thermo Fisher Scientific). Samples were spun in an Eppendorf microcentrifuge at 12,000g for 10 min, and 20 μL of supernatant were used for quantification. The accumulation of DA in the absence of the decarboxylase inhibitor NSD-1015 and of L-DOPA in the presence of 100 μM NSD-1015 was quantified by HPLC with coulometric detection (HPLC-EC) as previously described (González-Sepúlveda et al., 2022). The chromatography system consisted of a reverse-phase C18 column (2.5-μm particle Fortis C18, 10 × 0.46 cm, Sugelabor; Spain) and an ion-pair mobile phase, made up of 50 mM citric acid buffer, 0.05 mM EDTA, 1.2 mM octanesulfonic acid (pH 2.8) plus 1% (v/v) methanol. The injection loop volume was 100 μL and the flow rate was 1 mL/min. Concentrations of L-DOPA, DA and DOPAC were detected with a Coulochem II (ESA) detector with a model 5011 dual-electrode analytical cell with porous graphite electrodes. The potential of electrodes 1 and 2 was set at −0.05 V and +0.4 V, respectively. Standards of L-DOPA, DA and DOPAC at different concentrations (0.05–5 pmol/μL) were injected in every experiment to quantify the three catechol substances by the external standard method. The obtained concentrations were corrected by protein content in each sample.

In the experiments on exogenous dopamine uptake, the striatal minces were incubated, in Krebs-Ringer buffer, with tetrabenazine 1 μM for 1h at 37 °C, with CHIR99021 30 μM or with Krebs-Ringer buffer alone (as control). Additionally, a group of samples was kept in ice, to measure the basal levels prior to treatment. At the midpoint of TBZ and CHIR99021 incubations (i.e., 30 min from the addition of the compounds), DA 5 μM was also added and left to proceed for 30 min more. The amounts of DA and of DOPAC inside tissue were determined at the end of the incubations in every case by HPLC (as pmol DA/mg protein, 6

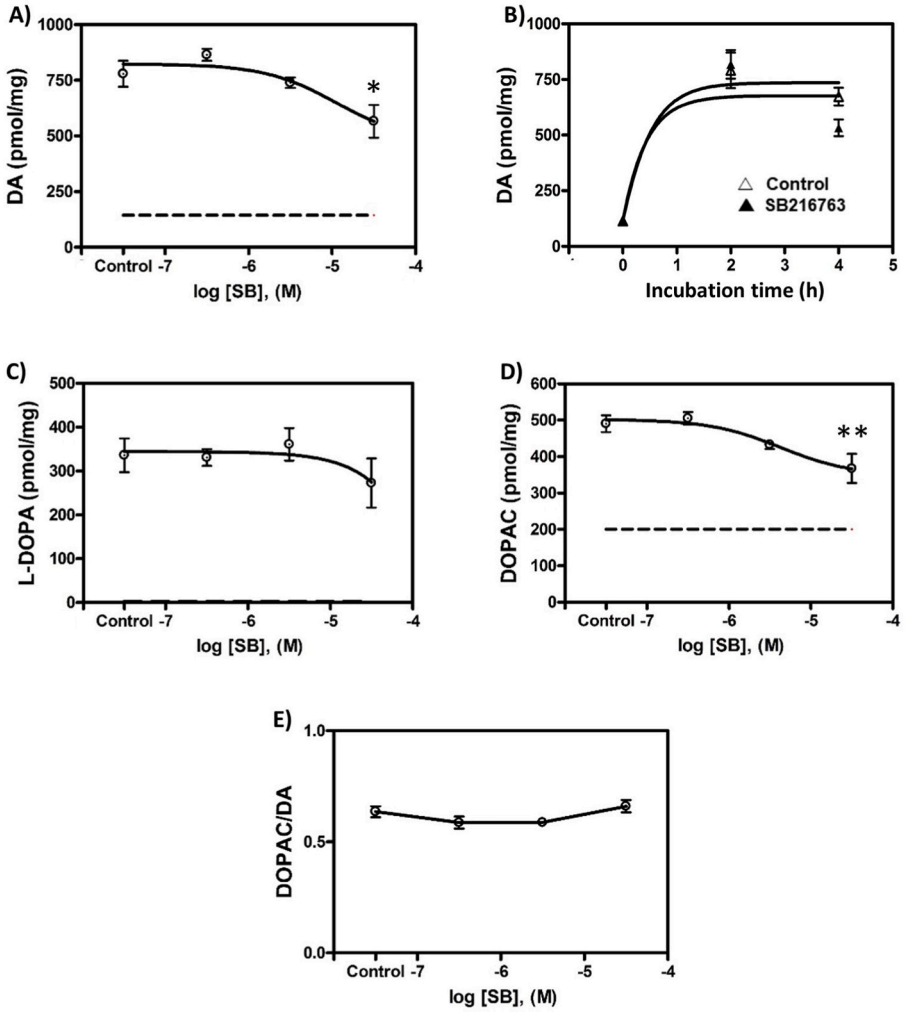

Fig. 3. Effect of SB216763 on dopamine accumulation and metabolism in rat brain striatal minces. (A) Concentration-response curve of SB216763, measuring dopamine (DA) accumulation over an incubation period of 2 h *ex vivo*, using concentrations of 0.3, 3 and 30 μM SB216763 or control without SB217663 (six incubates per group obtained from a single animal, n = 6). Basal dopamine was measured as control samples placed on ice during the 2h incubation period (six incubates, dashed line). **(B)** Time-response curve of DA accumulation on striatal minces *ex vivo* for a SB216763 concentration of 3 μM and for two and 4 h (n = 6, black triangles), and controls (n = 6, white triangles) for each incubation period, which were treated with the corresponding concentration of vehicle (DMSO), and basal dopamine measured the same as in (A) and represented as 0 time (n = 6). The same protocol as in A was used in striatal minces to determine L-DOPA **(C)** and DOPAC levels **(D)**. The DOPAC/DA ratio was calculated **(E)**. Data are expressed as mean ± SEM for each group, SB216763 vs control, one-way ANOVA followed by Dunnett's post-hoc test for dose-response graph and two-way ANOVA followed by Bonferroni's post-hoc test for time-response graph. *p < 0.5, **p < 0.01. Sigmoidal dose-response curve regression was used in every case to create the adjusted curves.

incubates per group obtained from a single animal).

2.4. Newly-synthesized [^{3}H]-DA determination by HPLC-UV

[^{3}H]-Tyrosine was purified as described previously (González-Sepúlveda et al., 2022). The concentration-response curve of CHIR99021 on striatal [^{3}H]-DA synthesis in minces *ex vivo* was measured (as in the *Preparation of striatal minces* Section). Prior to compound addition, a preincubation period of 2h was performed when stated, to assure stabilization of tissue metabolism. CHIR was added using concentrations of 0.3, 3 and 30 μM (n = 6 per concentration) or control without CHIR (n = 6) 10 min before the end of preincubation. Then, 0.12 μM purified [^{3}H]-tyrosine was added and incubated for 10 additional minutes and [^{3}H]-DA synthesis was stopped by the addition of 25 μL of a deproteinizing mixture containing trichloroacetic acid (0.5% w/v), 1 mM ascorbic acid and 25 nmol DA (as internal standard). Samples were homogenized in a Dynatech/Sonic Dismembrator (Dynatech Labs; Chantilly, VA) and protein quantification was assessed by the BCA method (Thermo Fisher Scientific). After centrifugation of the tissue homogenates (12,000g, 10 min, 4 °C), all supernatants were processed for [^{3}H]-DA purification by HPLC-UV. [^{3}H]-DA formed during the incubation reaction was separated from [^{3}H]-tyrosine by HPLC consisting of a reverse-phase C18 column (Tracer Extrasil ODS2, 5-μm particle size, 25 × 0.46 cm, Teknokroma; Spain) and an ion-pair mobile phase (100 mM sodium phosphate buffer, 1 mM EDTA, 0.75 mM octanesulfonic acid (pH 5) plus 12% (v/v) methanol) with a flow rate of 1 mL/min. This procedure was according to Ortiz et al. (2000), and to Ma et al. (2014). Internal standard DA was detected by UV 285 nm. Purified samples contained undetectable levels of radiolabeled tyrosine. Similarly, endogenous tyrosine and DA were undetectable and negligible, as compared to the amounts of internal standard DA used. The recovery of the internal standard in each sample (internal/external standard peak area) was quantified from internal standard DA HPLC-UV peak areas. [^{3}H]-DA was determined by sampling fractions (2 mL) of the DA peak, mixed with 6 mL of a Optiphase HiSafe III cocktail, and quantified in a liquid scintillation counter (Perkin Elmer Tri-Carb 2810 TR; USA). DA internal standard recovery and dpm in blank samples were used to correct the disintegrations per minute (dpm) obtained in HPLC-purified

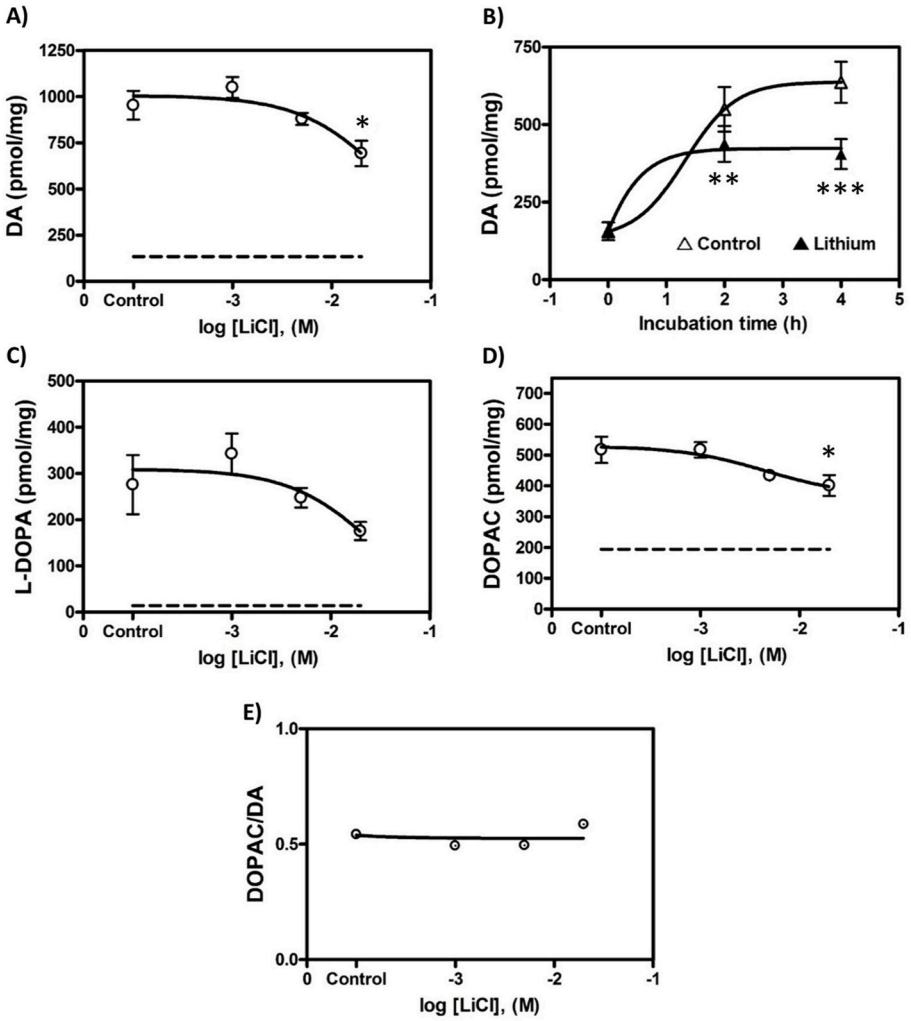

Fig. 4. Effect of lithium ion on dopamine accumulation and metabolism in rat brain striatal minces. (A) Concentration-response curve of lithium, measuring DA accumulation over an incubation period of 2 h *ex vivo*, using concentrations of 1, 5 and 20 mM LiCl or control without lithium (six incubates per group obtained from a single animal, n = 6). Basal DA was measured as control samples placed on ice during the 2h incubation period (six incubates, dashed line). **(B)** Time-response curve of DA accumulation on striatal minces *ex vivo* for a lithium concentration of 20 mM for two and 4 h (n = 6, black triangles), and controls (n = 6, white triangles) for each incubation period, which were treated with vehicle. Basal DA was measured the same as in (A) and represented as 0 time (n = 6). The same protocol as in A was used in striatal minces to determine L-DOPA **(C)** and DOPAC levels **(D)**. The DOPAC/DA ratio was calculated **(E)**. Data are expressed as mean ± SEM for each group, lithium vs control, one-way ANOVA followed by Dunnett's post-hoc test for dose-response graph and two-way ANOVA followed by Bonferroni's post-hoc test for time-response graph. *p < 0.5, **p < 0.01, ***p < 0.001. Sigmoidal dose-response curve regression was used in every case to create the adjusted curves.

[^{3}H]-DA fractions. The rate of [^{3}H]-DA synthesis was estimated as the ratio of corrected dpm divided by protein content in each incubate and the incubation time in the presence of [^{3}H]-tyrosine. Results were expressed as a percentage with respect to control samples run in the same experiment.

2.5. Tyrosine Hydroxylase activity in homogenates obtained from striatum

Striata from a single rat were extracted and placed in 5 mL of cold sodium phosphate buffer 10 mM pH 7.4 and homogenized using a glass Potter homogenizer. Two-hundred μL of homogenates were distributed in incubation tubes in the absence or presence of increasing concentrations of CHIR99021. Then, 100 μM NSD-1015, 30 μM tyrosine and 100 μM tetrahydrobiopterin (BH_4) were added. After 30 min of incubation at 37 °C, samples were placed in an ice block and 25 μL of a deproteinizing mixture (containing 0.5% w/v trichloroacetic acid) were added. Samples were centrifuged at 10,000g for 10 min and supernatants injected into HPLC-ECD to quantify L-DOPA and expressed as L-DOPA pmol/mg protein.

2.6. Western blot

After incubation of striatal minces as described above, Krebs-Ringer buffer was removed by centrifugation and tissue was homogenized in 1% SDS. Protein amount was determined by the BCA method. Samples from every treatment and with the same amount of total protein were separated by SDS-PAGE and transferred to polyvinylidene fluoride membranes in a Trans-Blot Turbo Transfer System (Bio-Rad). The composition of the blotting buffer was 25 mM Tris, 200 mM glycine and 10% methanol (v/v). Protein-containing membranes were incubated for 1h with Tris-buffered saline, supplemented with 0.1% Tween 20 and 5% (w/v) defatted powdered milk. Subsequently, the membranes were incubated overnight with primary antibody diluted in blocking buffer. The antibody from rabbit against β-catenin with triple phosphorylation in residues Ser33, Ser37 and Thr41 was from Invitrogen (PA5-67518, used at 1:1,000), while the mouse antibody against total β-catenin was from Transduction Laboratories (BD610154, used at 1:1,000). The primary antibodies against TH (AB5280, used at 1:2,500), TH phosphorylated at serine 31 (AB5423, used at 1:1,000) and TH phosphorylated at serine 40 (AB5935, used at 1:1,000) were obtained from Millipore. The

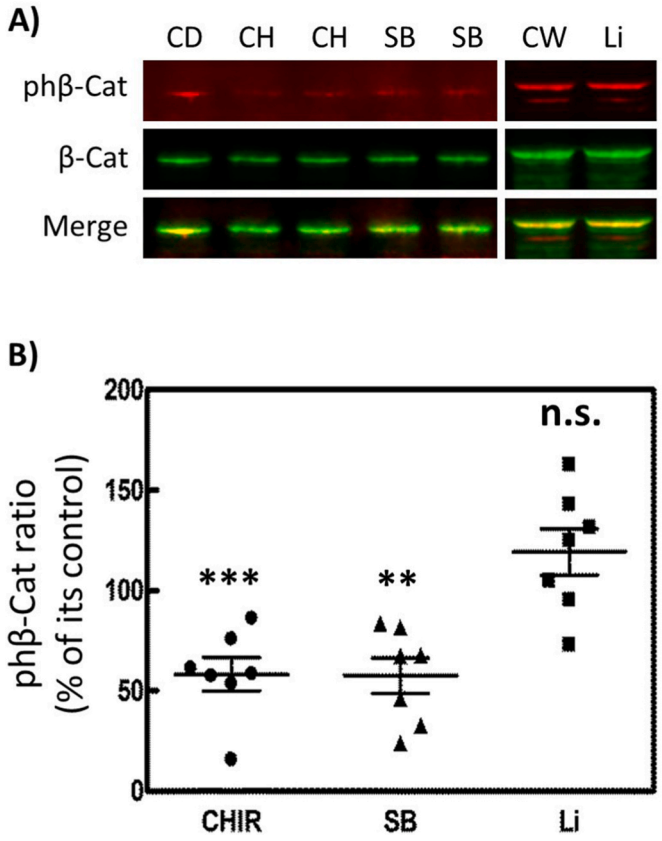

Fig. 5. GSK3β inhibitors CHIR99021 and SB216763, but not lithium, cause decrease in phosphorylation of β-catenin in rat striatal minces. Tissue samples were treated with two GSK3 inhibitors, CHIR99021 (CH, 3 μM) or SB216763 (SB, 3 μM), both for 2h. In parallel, striatal minces were also treated with lithium chloride (Li, 5 mM) for 2h. Levels of phosho-β-catenin were assessed with western blot using Near IR-labeled secondary antibodies, as described in the Materials and Methods section. **(A)** Representative western blots are shown after CHIR99021, SB216763 or lithium treatment. The red signal corresponds to β-catenin triple phosphorylated in S33, S37 and T41, while the green signal corresponds to total β-catenin. The merging of both signals appears in yellow. Control with only DMSO as vehicle was used in the cases of CHIR99021 and SB216763 (shown as CD), while control with water as the vehicle was used in the case of lithium (shown as CW). **(B)** Scatter plot representation of the β-catenin phosphorylation ratios (phosphorylated over total) after treatment with CHIR99021, SB216763 or lithium. Each point corresponds to the percentage of the ratio, with respect to its control (CD or CW). Graphics shows mean ± SEM, after one-way ANOVA analysis with the Newman-Keuls post-test. (**p < 0.01, ***p < 0.001, n.s. non-significant).

antibody against TH phosphorylated at serine 19 (AB5935, used at 1:1,000) was obtained from Thermo Fisher Scientific. The secondary antibodies were IRDye 800CW donkey anti-mouse and IRDye 680RD donkey anti-rabbit (Li-Cor) and were used at 1:10,000 in blocking buffer supplemented with 0.01% SDS, for 1h at room temperature in the dark. Infra-red signals were visualized using an Odyssey Fc Infrared Imaging System (Li-Cor). Total and phosphorylated forms were evaluated on the same membrane and the signals were acquired and quantified with Image Studio Lite software. The ratios of phosphorylated to total protein were calculated, with respect to controls, which were arbitrarily set to 100%.

2.7. Statistical Analysis

Graphs represent incubation samples that may be obtained from different animals, which is important due to the limited amount of brain striatal tissue per animal and its inherent heterogeneity. The use of the term "replicates" has been avoided to stress the heterogeneity of tissue minces randomly assigned to each treatment group. Statistical analysis was carried out with GraphPad Prism9 software (GraphPad Software Inc.; USA). Two-way ANOVA was used to analyze the interaction between different factors on synthesis rate (e.g., time, treatment, or concentration of DA as factors). Statistical significance of differences vs. control group was assessed by one-way ANOVA followed by Dunnett's post-hoc test for dose-response graphs and two-way ANOVA followed by Bonferroni's post-hoc test for time-response graphs. A sigmoidal dose-response curve regression was used in every case to create the adjusted curves. One-way ANOVA analysis with the Newman-Keuls post-test was used in the rest of the experiments.

3. Results

3.1. CHIR99021 strongly decreases endogenous dopamine accumulation and TH activity in rat striatal minces

With the aim of analyzing the effect of CHIR99021 on DA accumulation, striatal minces were treated with three different concentrations (0.3, 3 and 30 μM) over an incubation period of 2 h. A concentration-dependent decay in DA accumulation, with an IC_{50} of 3.76 μM, can be clearly observed (Fig. 1A). In fact, the 30 μM concentration was even able to decrease accumulation to the basal level (dashed line), which represents non-incubated tissue kept on ice. A time-dependent effect of CHIR99021 at 3 μM on DA accumulation was also observed (Fig. 1B). To further investigate DA metabolism, we also determined the levels of DOPAC and the DOPAC/DA ratio in the presence of growing concentrations of CHIR99021, as the DOPAC/DA ratio is considered to reflect the degree of DA metabolization by monoamine oxidase (MAO). While no significant changes in DOPAC levels were found (Figure 1C), a dramatic increase in the DOPAC/DA ratio was detected at 30 μM CHIR99021 (Fig. 1D), due to DA decrease. This suggests either an increased DA metabolism or a decreased TH activity.

Thus, to assess the effect of CHIR99021 on TH activity, striatal minces or homogenates were incubated in the presence of 100 μM NSD-1015 to inhibit L-aromatic amino-acid decarboxylase allowing the quantification of L-DOPA accumulation. While CHIR99021 induced a concentration-dependent inhibition of TH activity in striatal minces with an IC_{50} of 8.16 μM (Fig. 1E), no effect of CHIR99021 on TH was observed in striatal homogenates (Fig. 1F). These results suggest that the decrease of L-DOPA levels is not a result from direct interaction of CHIR99021 with TH and, therefore, the intact intracellular machinery is required.

Since DA accumulation is a result of new DA synthesis and storage, it was decided to test the effect of CHIR99021 on newly synthesized DA using a radioisotopic method to measure [^{3}H]-DA synthesis from [^{3}H]-tyrosine in striatal minces. CHIR99021 decreased concentration-dependent [^{3}H]-DA synthesis (Fig. 2A), as in the case of DA accumulation. In this case, the value of IC_{50} obtained was approximately 0.30 μM. Western blots against TH were performed to determine whether the decrease in DA synthesis was due to a decrease in the amount of TH protein. This was not altered under any of the CHIR concentrations tested, either in absolute values or in relation to GAPDH (Fig. 2B). Thus, the abrogation of the TH activity by CHIR is not due to a loss of TH protein but rather to a regulatory mechanism affecting efficiency of the enzyme.

3.2. SB216763 and lithium ion do not decrease dopamine content or alter DA metabolism

To corroborate a role of GSK3β in the decrease of TH activity and DA accumulation, another GSK3β inhibitor called SB216763 was also tested. SB216763 was able to slightly decrease dopamine accumulation in rat striatal minces over a 2-h period, but only at 30 μM (Fig. 3A) and had no effect at 3 μM or 0.3 μM, even after 4 h of incubation (Fig. 3B).

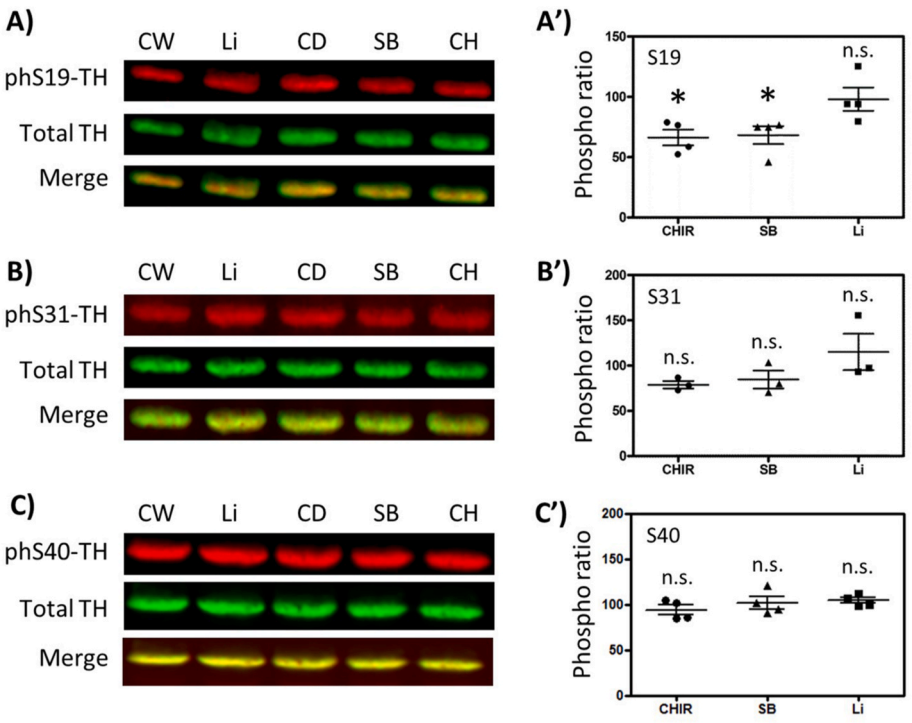

Fig. 6. GSK3 inhibitors decrease phosphorylation of Tyrosine Hydroxylase in Ser19, but not in Ser31 or Ser40. Samples from rat striatal minces were treated for 2 h with CHIR99021 (CH, 3 μM), SB216763 (SB, 3 μM), lithium chloride (Li, 5 mM), DMSO (control for CH99021 and SB216763, shown as CD) and water (control for LiCl, shown as CW). Phosphorylation in every case was assessed by western blot and NIR-labeled secondary antibodies. The red signal corresponds to phosphorylated TH, the green signal corresponds to total TH, while the merging of both signals appears in yellow. Representative western blots of phosphorylated TH in Ser19 **(A)**, Ser31 **(B)** and Ser40 **(C)**, after treatment with CHIR99021, SB216763 and lithium ion are shown. Next to each group of western blots, the corresponding Scatter plot representations of every phosphorylation ratio (phospho-TH signal over total TH signal) are shown, in percentage, with respect to its respective control **(A′, B′ and C′)**. Graphics show mean ± SEM, after one-way ANOVA analysis with the Newman-Keuls post-test. (*$p < 0.5$, n.s. non-significant).

The assessment of TH activity by L-DOPA quantification showed a lack of action by SB216763 at every concentration tested (Fig. 3C). Quantification of DOPAC levels at increasing concentrations of SB216763 showed a similar profile as that of DA accumulation shown in 3A, with only a slight decrease of the DOPAC amount at 30 μM (Fig. 3D), thus yielding a DOPAC/DA ratio unaltered, with respect to control, at any SB216763 concentration (Fig. 3E). Given that lithium chloride has antipsychotic properties and has also been reported to inhibit GSK3, the effects of lithium ion on DA metabolism in striatal minces were also tested. It was observed that 20 mM LiCl yielded a significant but slight decrease in DA accumulation over a 2-h incubation period, whereas no effect was detected at 1 or 5 mM (Fig. 4A). A time-course with 20 mM lithium showed significant decreases in DA accumulation after two and 4 h of incubation (Fig. 4B). Determinations of L-DOPA (Fig. 4C), DOPAC (Fig. 4D) and the DOPAC/DA ratio (Fig. 4E) at 1, 5, or 20 mM lithium for 2h did not show remarkable changes, with respect to control.

3.3. CHIR99021 and SB216763, but not lithium, inhibit GSK3β activity on β-catenin in striatum minces

GSK3β phosphorylates β-catenin in residues S33, S37 and T41. Thus, to directly test the inhibitory effect of CHIR99021, SB216763 and of lithium on the GSK3β activity in our system, the amount of triple phosphorylated β-catenin was assessed by western blot. Near infrared-labeled secondary antibodies were used, thus phosphorylated and total protein levels could be assessed in the same membrane, giving rise to reliable signal quantifications. Treatment with 3 μM CHIR99021 and with 3 μM SB216763 for 2h decreased GSK3β-phosphorylated β-catenin by half, approximately, whereas 5 mM lithium for 2h did not show any effect on β-catenin phosphorylation (Fig. 5A and B). These results corroborate that CHIR99021 and SB216763 cause inhibition of GSK3β in our striatal minces. In consequence, the lack of any SB216763 effect on DA metabolism is due to the absence of GSK3β action on TH and not to a lack of compound efficacy.

3.4. CHIR99021 and SB216763 decrease TH phosphorylation in serine 19, but not in serines 31 and 40

Since phosphorylation in serine residues have been described as a regulatory event of TH activity, the effect of CHIR99021 on TH phosphorylation was explored. Western blots with phosphospecific antibodies showed that GSK3β inhibition causes significant decrease of TH phosphorylation in serine 19, approximately 30% after CHIR99021 or SB216763 treatment for 2h (Fig. 6A and A′). On the other hand, no changes in phosphorylation were detected in either serine 31 or in serine 40 (Fig. 6B, B′, 6C and 6C'). Treatment with LiCl (5 mM for 2h) did not yield any change in any of the tested phosphosites.

3.5. CHIR99021 impairs the accumulation of exogenous DA into striatal minces

To further explore the mechanisms that lead to the dramatic action of CHIR99021 on DA accumulation, the effect of CHIR99021 on DA transport into striatal tissue was tested. Striatal minces were incubated with 5 μM DA in the absence or presence of CHIR99021 30 μM or of tetrabenazine (TBZ) 1 μM, a VMAT2 inhibitor, and the amount of DA incorporated inside tissue was determined by HPLC, as well as the amount of DOPAC (Fig. 7A). The rationale behind the use of TBZ derives from published results from our group (González-Sepúlveda et al., 2022) in which TBZ showed clear similarities with the effect of CHIR99021 on DA accumulation described in the present work. Incubation of minces with exogenously added DA caused a large increase in the DA found in

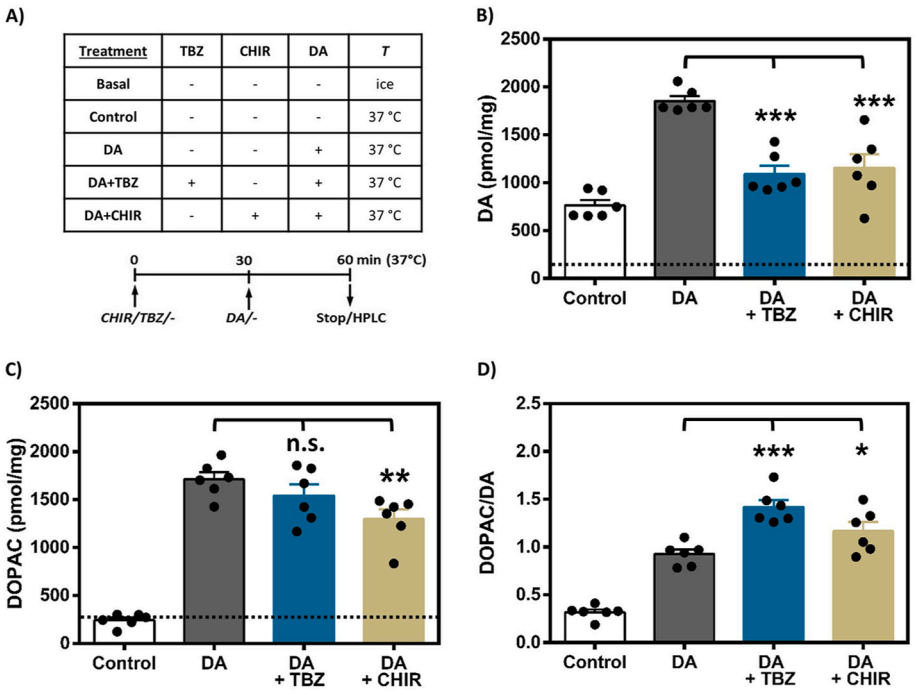

Fig. 7. CHIR99021 decreases dopamine storage inside rat brain striatal minces. (A) Striatal minces were incubated for 1 h in ice (Basal) or at 37 °C with tetrabenazine 1 μM (TBZ), with CHIR99021 30 μM (CHIR) or with Krebs-Ringer buffer (−). For the last 30 min of incubation 5 μM DA was also added, except in the Basal and Control samples. The amount of DA **(B)** and of DOPAC **(C)** inside tissue was determined at the end of the incubations in every case by HPLC (as pmol DA/mg protein, six incubates per group obtained from a single animal). Basal DA or DOPAC in untreated samples is indicated in both cases as dashed lines. Control samples were incubated at 37 °C without any drug or DA. The DA turnover was also determined in every case as DOPAC/DA ratios **(D)**. Data are expressed as mean ± SEM for each group. The one-way ANOVA test was performed followed by the Newman-Keuls post-test vs the DA treatment alone (DA) when indicated (n.s., non-significant, *$p < 0.5$, **$p < 0.01$, ***$p < 0.001$).

the tissue, which is interpreted as DA incorporation into tissue, mainly synaptic vesicles, thanks to VMAT2 activity. Pretreatment with either CHIR99021 or TBZ similarly caused a clear reduction (≈70%) of the DA additionally incorporated into tissue, with respect to the control situation (Fig. 7B). On the other hand, the assessment of DOPAC levels showed a large increase after DA incubation, but they were poorly or non-modified after TBZ or CHIR99021 pretreatment (Fig. 7C). The DOPAC/DA ratios after every treatment were also assessed (Fig. 7D), showing that DA turnover is moderately increased by TBZ and CHIR909021 when exogenous DA is present. These results point to an effect of CHIR99021 on some component of the DA transport or storage inside cells.

3.6. Tetrabenazine strongly decreases endogenous dopamine accumulation

Since previous work from our group had shown that TBZ dramatically decreases the rate of DA synthesis (González-Sepúlveda et al., 2022) in a strikingly similar way to what CHIR99021 does, the same experiments as those shown in Fig. 1 were additionally conducted with different concentrations of TBZ. The results also showed a strong decrease in DA accumulation at the highest TBZ concentrations used (0.05, 0.1 and 1 μM) for 2h, even below the basal level (Fig. 8A). The sigmoidal curve response obtained after TBZ treatment yielded an IC_{50} of 41.3 nM on DA accumulation. On the other hand, the DOPAC levels remain with no or small changes, showing a modest increase at the highest concentration of TBZ used (1 μM, Fig. 8B). These results yielded a ten-fold increase in the DOPAC/DA ratio (Fig. 8C), which indicates an increased DA metabolism or a decreased TH activity in the same way that is seen with CHIR99021 (Fig. 1).

4. Discussion

CHIR99021 is a small organic molecule that potently inhibits GSK3α (IC_{50}∼10 nM) and GSK3β (IC_{50}∼5 nM) with high selectivity and is considered the standard activator of the Wnt/β-catenin pathway (Bennett et al., 2002). Moreover, it is a compound that has been tested in a plethora of pathologies (Badimon et al., 2019; Oh et al., 2017; Lee et al., 2018; Houben et al., 2022; Uhl et al., 2015; Zhao et al., 2014; Ring et al., 2003), showing pharmacological potential in some of them. Furthermore, treatment of isolated rat pancreatic islets with CHIR99021 or SB216763 increases the rate of beta-cell replication (Mussmann et al., 2007). Even though CHIR99021 is considered the gold standard for GSK3β inhibition, its off-target effects have been demonstrated. A report describes some action of CHIR99021 on more than 20 kinases as well as the existence of more specific GSK3 inhibitors (An et al., 2012). These off-target effects have been highlighted by a recent report showing that CHIR99021 causes, independently of GSK3, the suppression of the proteasomal degradation of CAST and of the related calpain activity (Hu et al., 2021). This suppression leads to a great enhancement of the mitochondrial function by impairing the action of the GTPase dynamin-related protein 1 (Drp1) on mitochondrial fragmentation. The authors hypothesized that CHIR99021 suppresses CAST degradation through the inhibition of ubiquitin ligases or activation of deubiquitinases (Hu et al., 2021). Additionally, the promotion by CHIR99021 of mitochondrial biogenesis, oxidative phosphorylation, and the production of reactive oxygen species in human endodermal progenitor cells has also been observed, despite these effects being attributed to the GSK3/β-catenin pathway and not to off-target effects of CHIR99021 (Ma et al., 2019). No experiments involving mitochondria were conducted in the present work and no conclusions on this issue can be raised, but we consider that the effect of CHIR99021 on mitochondrial function in striatal tissue is a matter of interest.

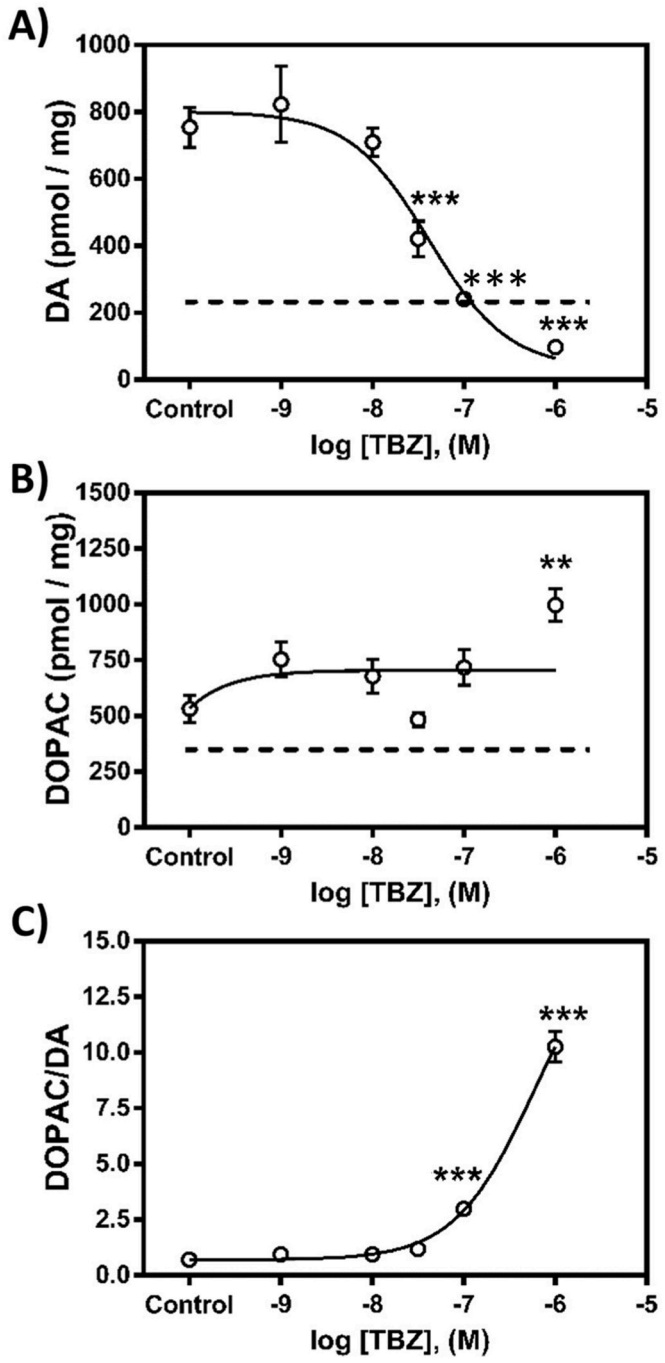

Fig. 8. Effect of tetrabenazine (TBZ) on endogenous dopamine accumulation and metabolism in rat brain striatal minces. Concentration-response curve of TBZ, measuring DA **(A)** or DOPAC **(B)** accumulation over an incubation period of 2 h *ex vivo*, using different TBZ concentrations (0.001, 0.01, 0.05, 0.1 and 1 μM) or control without TBZ (incubates per group obtained from two animals, n = 4–11). Basal DA was measured as control samples placed on ice during the 2-h incubation period (dashed lines). The DOPAC/DA ratio was calculated **(C)**. Data are expressed as mean ± SEM for each group, TBZ vs control, one-way ANOVA followed by Dunnett's post-hoc test for the dose-response graph and two-way ANOVA followed by Bonferroni's post-hoc test for the time-response graph. *$p < 0.5$, **$p < 0.01$, ***$p < 0.001$. Sigmoidal dose-response curve regression was used in every case to create the adjusted curves.

The feedback inhibition of DA synthesis by catecholamines, DA itself and also adrenaline and noradrenaline, has been described (Daubner et al., 2011). Computational analyses have indicated the potential importance of this feedback effect in dopaminergic neurotransmission (Wallace, 2007), while *ex vivo* experimental studies have recently revealed that spontaneous inhibition in DA synthesis appeared when storage reached saturation or is inhibited by TBZ, causing DA spillover and end-product feedback-inhibition of TH in living tissue (González-Sepúlveda et al., 2022). *In vitro* studies suggest the existence in TH of two DA binding sites with high and low affinities (K_D 4 nM and 90 nM, respectively) (Gordon et al., 2008; Nakashima et al., 2009; Dickson and Briggs, 2013; Tekin et al., 2014). The TH low-affinity site/conformation could act as a physiological sensor in the event that synaptic vesicles were filled with DA at its maximum capacity, since the surplus of the DA inside the cytosol of synaptic terminals would bind to the low-affinity site/conformation, causing inhibition of TH activity. In agreement with the role of DA in TH inhibition by CHIR99021 is the observation that the determination of the TH activity, assessed by means of the L-DOPA levels, under the presence of the decarboxylase inhibitor NSD-1015 (Fig. 1E) yielded an IC_{50} one order of magnitude higher than when TH activity was assessed by ^{3}H-DA production (Fig. 2A). Thus, the enabling of DA production potentiates the depleting effect of CHIR99021 in terms of efficacy. Additionally, TH feedback inhibition by other catecholamines cannot be discarded.

Regarding the effect of both CHIR99021 and of SB216763 on TH phosphorylation, Ser19 is reported to be phosphorylated in a 14-3-3 dependent manner and has little effect on the activity of TH *in vitro* (Itagaki et al., 1999; Toska et al., 2002). Phosphorylation of TH in Ser19 is related to enzyme degradation of the enzyme by proteasome (Nakashima et al., 2016). The interaction with 14-3-3 proteins, mainly with the γ isoform (Halskau et al., 2009), reduces the sensitivity of phosphorylated human TH isoform 1 to proteolysis by protecting its N-terminal part (Obsilova et al., 2008). Despite these results, the dramatic abrogation of TH activity shown in the present work cannot be caused by loss of TH protein, since its levels remain unaltered after CHIR99021 treatment, nor to the relatively small change in phosphoSer19.

One relevant finding of the present work is the dramatic increase of the DOPAC/DA ratio caused by CHIR99021 (Fig. 1D), very similar to that caused by TBZ (Fig. 8C). This result can be explained by the enhancement of the MAO activity triggered by the accumulation of its substrate, i.e., DA in the cytosol of the synaptic terminal. This DA accumulation would lead to the inhibition of TH by a feedback effect, as has been described by our group (González-Sepúlveda et al., 2022) and previously mentioned.

Even though the comparison between the effects of CHIR99021 and the effects of TBZ on the transport and metabolism of DA in striatal minces shows relevant similarities (Figs. 1, Figs. 7 and 8), more experiments are needed to explore the possibility that CHIR99021 exerts an off-target inhibitory effect on VMAT2, besides acting as a GSK3β inhibitor. Thus, no direct link between CHIR99021 and VMAT2 can be claimed in the basis of the results shown in the present work.

Since the main portion of the DA in the nerve terminal resides inside synaptic vesicles, where it is protected from metabolism prior to their synaptic release, we can assume that most of the DA incorporated into striatal minces directly reflects the amount of DA inside synaptic vesicles. TBZ is used for the treatment of the motor symptoms in Huntington's disease (HD), a fatal neurodegenerative disorder, and other hyperkinetic disorders (Jankovic, 2009), but it can cause side-effects, like nausea, difficulty in speaking, severe muscle stiffness or, even, depression (Jankovic, 2016). In any case, the reduction of DA release in the motor striatum by VMAT2 inhibition is considered a good therapeutic approach to reduce the involuntary hyperkinetic movements of tardive dyskinesia (Stahl, 2018). In fact, CHIR99021 showed to potently improve mitochondrial function and enhance cell viability in several models of HD (Hu et al., 2021). Thus, an available option to TBZ in the hands of the doctors would be a benefit in cases with severe side-effects,

and CHIR99021 appears as a candidate to also be used in HD or other movement pathologies, such as tardive dyskinesia or Tourette syndrome. Nevertheless, the exact mechanism of CHIR99021-mediated TH inhibition and DA depletion has not been elucidated and experiments focusing on the direct effect of CHIR99021 on vesicular transport are necessary.

CRediT authorship contribution statement

Sally Hamdon: Methodology, Investigation, Formal analysis, Writing – original draft, Visualization. **Pol Fernandez-Gonzalez:** Methodology, Investigation, Formal analysis. **Muhammad Yusof Omar:** Methodology, Investigation, Formal analysis. **Marta González-Sepúlveda:** Visualization, Formal analysis, Writing – original draft. **Jordi Ortiz:** Conceptualization, Validation, Formal analysis, Writing – original draft, Visualization, Supervision, Project administration, Funding acquisition. **Carles Gil:** Conceptualization, Validation, Formal analysis, Writing – original draft, Visualization, Supervision, Project administration, Funding acquisition.

Declaration of competing interest

The authors declare that they have no known competing financial interests or personal relationships that could have appeared to influence the work reported in this paper.

Data availability

No data was used for the research described in the article.

Acknowledgements

This work was supported by Spanish Government grant SAF2017-87199-R. S.H. received a predoctoral fellowship from the Universitat Autònoma de Barcelona. We thank the skillful technical assistance of Susana Benítez. We would also like to thank Mr. Chuck Simmons for the language revision of this manuscript.

Appendix A. Supplementary data

Supplementary data to this article can be found online at https://doi.org/10.1016/j.neuropharm.2023.109759.

References

An, W.F., Germain, A.R., Bishop, J.A., et al., 2012. Discovery of potent and highly selective inhibitors of GSK3β. In: Probe Reports from the NIH Molecular Libraries Program. National Center for Biotechnology Information (US), Bethesda (MD) [Internet]. https://www.ncbi.nlm.nih.gov/books/NBK133436/.

Badimon, L., Casaní, L., Camino-Lopez, S., Juan-Babot, O., Borrell-Pages, M., 2019. GSK3β inhibition and canonical Wnt signaling in mice hearts after myocardial ischemic damage. PLoS One 14 (6), e0218098. https://doi.org/10.1371/journal.pone.0218098.

Bennett, C.N., Ross, S.E., Longo, K.A., Bajnok, L., Hemati, N., Johnson, K.W., Harrison, S. D., MacDougald, O.A., 2002. Regulation of Wnt signaling during adipogenesis. J. Biol. Chem. 277 (34), 30998–31004. https://doi.org/10.1074/jbc.M204527200.

Bibb, J.A., 2005. Decoding dopamine signaling. Cell 122 (2), 153–155. https://doi.org/10.1016/j.cell.2005.07.011.

Bird, E.D., Spokes, E.G., Iversen, L.L., 1979. Increased dopamine concentration in limbic areas of brain from patients dying with schizophrenia. Brain: J. Neurol. 102 (2), 347–360. https://doi.org/10.1093/brain/102.2.347.

Bobrovskaya, L., Gilligan, C., Bolster, E.K., Flaherty, J.J., Dickson, P.W., Dunkley, P.R., 2007. Sustained phosphorylation of tyrosine hydroxylase at serine 40: a novel mechanism for maintenance of catecholamine synthesis. J. Neurochem. 100 (2), 479–489. https://doi.org/10.1111/j.1471-4159.2006.04213.x.

Daubner, S.C., Le, T., Wang, S., 2011. Tyrosine hydroxylase and regulation of dopamine synthesis. Arch. Biochem. Biophys. 508 (1), 1–12. https://doi.org/10.1016/j.abb.2010.12.017.

Dickson, P.W., Briggs, G.D., 2013. Tyrosine hydroxylase: regulation by feedback inhibition and phosphorylation. Adv. Pharmacol. 68, 13–21. https://doi.org/10.1016/B978-0-12-411512-5.00002-6.

Duda, P., Hajka, D., Wójcicka, O., Rakus, D., Gizak, A., 2020. GSK3β: a master player in depressive disorder pathogenesis and treatment responsiveness. Cells 9 (3), 727. https://doi.org/10.3390/cells9030727.

Dunkley, P.R., Dickson, P.W., 2019. Tyrosine hydroxylase phosphorylation in vivo. J. Neurochem. 149 (6), 706–728. https://doi.org/10.1111/jnc.14675.

Gonzalez-Sepulveda, M., Compte, J., Cuadros, T., Nicolau, A., Guillard-Sirieix, C., Peñuelas, N., Lorente-Picon, M., Parent, A., Romero-Giménez, J., Cladera-Sastre, J. M., Laguna, A., Vila, M., 2023. In vivo reduction of age-dependent neuromelanin accumulation mitigates features of Parkinson's disease. Brain: J. Neurol. 146 (3), 1040–1052. https://doi.org/10.1093/brain/awac445.

González-Sepúlveda, M., Omar, M.Y., Hamdon, S., Ma, G., Rosell-Vilar, S., Raivio, N., Abass, D., Martínez-Rivas, A., Vila, M., Giraldo, J., Carrascal, M., Abián, J., Gil, C., Sabriá, J., Ortiz, J., Moreno-Delgado, D., 2022. Spontaneous changes in brain striatal dopamine synthesis and storage dynamics ex vivo reveal end-product feedback-inhibition of tyrosine hydroxylase. Neuropharmacology 212, 109058. https://doi.org/10.1016/j.neuropharm.2022.109058.

Gordon, S.L., Quinsey, N.S., Dunkley, P.R., Dickson, P.W., 2008. Tyrosine hydroxylase activity is regulated by two distinct dopamine-binding sites. J. Neurochem. 106 (4), 1614–1623. https://doi.org/10.1111/j.1471-4159.2008.05509.x.

Halskau Jr., Ø., Ying, M., Baumann, A., Kleppe, R., Rodriguez-Larrea, D., Almås, B., Haavik, J., Martínez, A., 2009. Three-way interaction between 14-3-3 proteins, the N-terminal region of tyrosine hydroxylase, and negatively charged membranes. J. Biol. Chem. 284 (47), 32758–32769. https://doi.org/10.1074/jbc.M109.027706.

Houben, R., Hesbacher, S., Sarma, B., Schulte, C., Sarosi, E.M., Popp, S., Adam, C., Kervarrec, T., Schrama, D., 2022. Inhibition of T-antigen expression promoting glycogen synthase kinase 3 impairs merkel cell carcinoma cell growth. Cancer Lett. 524, 259–267. https://doi.org/10.1016/j.canlet.2021.10.031.

Hu, D., Sun, X., Magpusao, A., Fedorov, Y., Thompson, M., Wang, B., Lundberg, K., Adams, D.J., Qi, X., 2021. Small-molecule suppression of calpastatin degradation reduces neuropathology in models of Huntington's disease. Nat. Commun. 12 (1), 5305. https://doi.org/10.1038/s41467-021-25651-y.

Itagaki, C., Isobe, T., Taoka, M., Natsume, T., Nomura, N., Horigome, T., Omata, S., Ichinose, H., Nagatsu, T., Greene, L.A., Ichimura, T., 1999. Stimulus-coupled interaction of tyrosine hydroxylase with 14-3-3 proteins. Biochemistry 38 (47), 15673–15680. https://doi.org/10.1021/bi9914255.

Jaber, M., Robinson, S.W., Missale, C., Caron, M.G., 1996. Dopamine receptors and brain function. Neuropharmacology 35 (11), 1503–1519. https://doi.org/10.1016/s0028-3908(96)00100-1.

Jankovic, J., 2009. Treatment of hyperkinetic movement disorders. Lancet Neurol. 8 (9), 844–856. https://doi.org/10.1016/S1474-4422(09)70183-8.

Jankovic, J., 2016. Dopamine depleters in the treatment of hyperkinetic movement disorders. Expet Opin. Pharmacother. 17 (18), 2461–2470. https://doi.org/10.1080/14656566.2016.1258063.

Johnson, M.E., Salvatore, M.F., Maiolo, S.A., Bobrovskaya, L., 2018. Tyrosine hydroxylase as a sentinel for central and peripheral tissue responses in Parkinson's progression: evidence from clinical studies and neurotoxin models. Prog. Neurobiol. 165–167, 1–25. https://doi.org/10.1016/j.pneurobio.2018.01.002.

Koob, G.F., Volkow, N.D., 2010. Neurocircuitry of addiction. Neuropsychopharmacology: official publication of the American College of Neuropsychopharmacology 35 (1), 217–238. https://doi.org/10.1038/npp.2009.110.

Lee, C., Robinson, M., Willerth, S.M., 2018. Direct reprogramming of glioblastoma cells into neurons using small molecules. ACS Chem. Neurosci. 9 (12), 3175–3185. https://doi.org/10.1021/acschemneuro.8b00365.

Lehmann, I.T., Bobrovskaya, L., Gordon, S.L., Dunkley, P.R., Dickson, P.W., 2006. Differential regulation of the human tyrosine hydroxylase isoforms via hierarchical phosphorylation. J. Biol. Chem. 281 (26), 17644–17651. https://doi.org/10.1074/jbc.M512194200.

Ma, G.F., Raivio, N., Sabrià, J., Ortiz, J., 2014. Agonist and antagonist effects of aripiprazole on D_2-like receptors controlling rat brain dopamine synthesis depend on the dopaminergic tone. Int. J. Neuropsychopharmacol. 18 (4) https://doi.org/10.1093/ijnp/pyu046 pyu046.

Ma, Y., Ma, M., Sun, J., Li, W., Li, Y., Guo, X., Zhang, H., 2019. CHIR-99021 regulates mitochondrial remodelling via β-catenin signalling and miRNA expression during endodermal differentiation. J. Cell Sci. 132 (15) https://doi.org/10.1242/jcs.229948 jcs229948.

Mackay, A.V., Iversen, L.L., Rossor, M., Spokes, E., Bird, E., Arregui, A., Creese, I., Synder, S.H., 1982. Increased brain dopamine and dopamine receptors in schizophrenia. Arch. Gen. Psychiatr. 39 (9), 991–997. https://doi.org/10.1001/archpsyc.1982.04290090001001.

McLean, W.J., Hinton, A.S., Herby, J., Salt, A.N., Hartsock, J.J., Wilson, S., Lucchino, D. L., Lenarz, T., Warnecke, A., Prenzler, N., Schmitt, H., King, S., Jackson, L.E., Rosenbloom, J., Atiee, G., Bear, M., Runge, C.L., Gifford, R.H., Rauch, S.D., Lee, D.J., Langer, R., Karp, J.M., Loose, C., LeBel, C., 2021. Improved speech intelligibility in subjects with stable sensorineural hearing loss following intratympanic dosing of FX-322 in a phase 1b study. Otol. Neurotol.: official publication of the American Otological Society, American Neurotology Society [and] European Academy of Otology and Neurotology 42 (7), e849–e857. https://doi.org/10.1097/MAO.0000000000003120.

Meiser, J., Weindl, D., Hiller, K., 2013. Complexity of dopamine metabolism. Cell Commun. Signal. 11, 34. https://doi.org/10.1186/1478-811X-11-34.

Mussmann, R., Geese, M., Harder, F., Kegel, S., Andag, U., Lomow, A., Burk, U., Onichtchouk, D., Dohrmann, C., Austen, M., 2007. Inhibition of GSK3 promotes replication and survival of pancreatic beta cells. J. Biol. Chem. 282 (16), 12030–12037. https://doi.org/10.1074/jbc.M609637200.

Nakashima, A., Hayashi, N., Kaneko, Y.S., Mori, K., Sabban, E.L., Nagatsu, T., Ota, A., 2009. Role of N-terminus of tyrosine hydroxylase in the biosynthesis of catecholamines. J. Neural. Transm. 116 (11), 1355–1362. https://doi.org/10.1007/s00702-009-0227-8. Vienna, Austria: 1996.

Nakashima, A., Ohnuma, S., Kodani, Y., Kaneko, Y.S., Nagasaki, H., Nagatsu, T., Ota, A., 2016. Inhibition of deubiquitinating activity of USP14 decreases tyrosine hydroxylase phosphorylated at Ser19 in PC12D cells. Biochem. Biophys. Res. Commun. 472 (4), 598–602. https://doi.org/10.1016/j.bbrc.2016.03.022.

Obsilova, V., Nedbalkova, E., Silhan, J., Boura, E., Herman, P., Vecer, J., Sulc, M., Teisinger, J., Dyda, F., Obsil, T., 2008. The 14-3-3 protein affects the conformation of the regulatory domain of human tyrosine hydroxylase. Biochemistry 47 (6), 1768–1777. https://doi.org/10.1021/bi7019468.

Oh, J., Kim, Y., Che, L., Kim, J.B., Chang, G.E., Cheong, E., Kang, S.G., Ha, Y., 2017. Regulation of cAMP and GSK3 signaling pathways contributes to the neuronal conversion of glioma. PLoS One 12 (11), e0178881. https://doi.org/10.1371/journal.pone.0178881.

Ortiz, J., Gómez, J., Torrent, A., Aldavert, M., Blanco, I., 2000. Quantitative radioisotopic determination of histidine decarboxylase using high-performance liquid chromatography. Anal. Biochem. 280 (1), 111–117. https://doi.org/10.1006/abio.2000.4494.

Ring, D.B., Johnson, K.W., Henriksen, E.J., Nuss, J.M., Goff, D., Kinnick, T.R., Ma, S.T., Reeder, J.W., Samuels, I., Slabiak, T., Wagman, A.S., Hammond, M.E., Harrison, S. D., 2003. Selective glycogen synthase kinase 3 inhibitors potentiate insulin activation of glucose transport and utilization in vitro and in vivo. Diabetes 52 (3), 588–595. https://doi.org/10.2337/diabetes.52.3.588.

Smith, J.S., Lefkowitz, R.J., Rajagopal, S., 2018. Biased signalling: from simple switches to allosteric microprocessors. Nat. Rev. Drug Discov. 17 (4), 243–260. https://doi.org/10.1038/nrd.2017.229.

Smith-Dijak, A.I., Sepers, M.D., Raymond, L.A., 2019. Alterations in synaptic function and plasticity in Huntington disease. J. Neurochem. 150 (4), 346–365. https://doi.org/10.1111/jnc.14723.

Spanagel, R., Weiss, F., 1999. The dopamine hypothesis of reward: past and current status. Trends Neurosci. 22 (11), 521–527. https://doi.org/10.1016/s0166-2236(99)01447-2.

Stahl, S., 2018. Mechanism of action of vesicular monoamine transporter 2 (VMAT2) inhibitors in tardive dyskinesia: reducing dopamine leads to less “go” and more “stop” from the motor striatum for robust therapeutic effects. CNS Spectr. 23 (1), 1–6. https://doi.org/10.1017/S1092852917000621.

Tekin, I., Roskoski Jr., R., Carkaci-Salli, N., Vrana, K.E., 2014. Complex molecular regulation of tyrosine hydroxylase. J. Neural. Transm. 121 (12), 1451–1481. https://doi.org/10.1007/s00702-014-1238-7. Vienna, Austria: 1996.

Tiger, G., Björklund, P.E., Cowburn, R.F., Fowler, C.J., 1989. Enhancement by potassium of carbachol-stimulated inositol phospholipid breakdown in rat cerebral cortical miniprisms: comparison with other depolarising agents. J. Neurochem. 52 (6), 1843–1853. https://doi.org/10.1111/j.1471-4159.1989.tb07266.x.

Toska, K., Kleppe, R., Armstrong, C.G., Morrice, N.A., Cohen, P., Haavik, J., 2002. Regulation of tyrosine hydroxylase by stress-activated protein kinases. J. Neurochem. 83 (4), 775–783. https://doi.org/10.1046/j.1471-4159.2002.01172.x.

Uhl, F.E., Vierkotten, S., Wagner, D.E., Burgstaller, G., Costa, R., Koch, I., Lindner, M., Meiners, S., Eickelberg, O., Königshoff, M., 2015. Preclinical validation and imaging of Wnt-induced repair in human 3D lung tissue cultures. Eur. Respir. J. 46 (4), 1150–1166. https://doi.org/10.1183/09031936.00183214.

Wallace, L.J., 2007. A small dopamine permeability of storage vesicle membranes and end product inhibition of tyrosine hydroxylase are sufficient to explain changes occurring in dopamine synthesis and storage after inhibition of neuron firing. Synapse 61 (9), 715–723. https://doi.org/10.1002/syn.20408.

Xu, B., Li, F., Zhang, W., Su, Y., Tang, L., Li, P., Joshi, J., Yang, A., Li, D., Wang, Z., Wang, S., Xie, J., Gu, H., Zhu, W., 2022. Identification of metabolic pathways underlying FGF1 and CHIR99021-mediated cardioprotection. iScience 25 (6), 104447. https://doi.org/10.1016/j.isci.2022.104447.

Zhao, J., Li, S., Trilok, S., Tanaka, M., Jokubaitis-Jameson, V., Wang, B., Niwa, H., Nakayama, N., 2014. Small molecule-directed specification of sclerotome-like chondroprogenitors and induction of a somatic chondrogenesis program from embryonic stem cells. Development 141 (20), 3848–3858. https://doi.org/10.1242/dev.105981.